AD-A162 339 A COMPREHENSIVE ANALYSIS ALGORITHM FOR ABLATION TEMPERATURE FIELDS AND TH..(U) FOREIGN TECHNOLOGY DIV WRIGHT-PATTERSON AFB OH Z HUANG 06 NOV 85 1/1

UNCLASSIFIED FTD-ID(RS)T-0701-85 F/G 7/4 NL

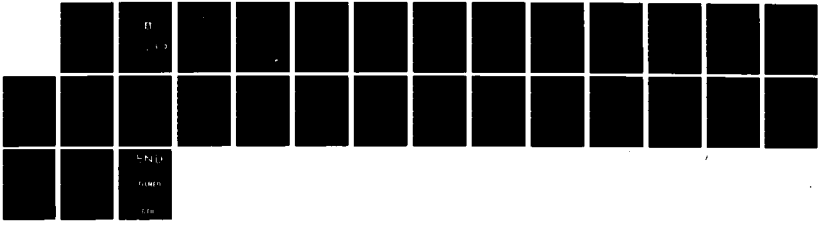

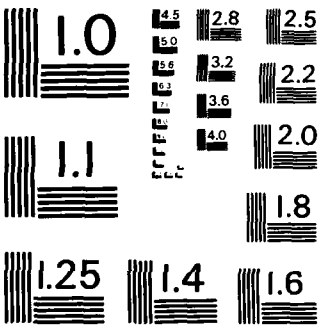

MICROCOPY RESOLUTION TEST CHART
NATIONAL BUREAU OF STANDARDS - 1963 - A

(2)

FTD-ID(RS)T-0701-85

FOREIGN TECHNOLOGY DIVISION

A COMPREHENSIVE ANALYSIS ALGORITHM FOR ABLATION, TEMPERATURE FIELDS, AND THERMAL STRESSES OF CARBON-BASED NOSETIP MATERIALS

by

Huang Zhenzhong

Approved for public release;
distribution unlimited.

A162 351

FTD-ID(RS)T-0701-85

EDITED TRANSLATION

FTD-ID(RS)T-0701-85 6 Nov 85

MICROFICHE NR: FTD-85-C-001029

A COMPREHENSIVE ANALYSIS ALGORITHM FOR ABLATION, TEMPERATURE FIELDS, AND THERMAL STRESSES OF CARBON-BASED NOSETIP MATERIALS--

By: /Huang Zhenzhong

English pages: 23

Source: Yuhang Xuebao, No. 3, 1984, pp. 30-38

Country of origin: China
Translated by: SCITRAN
F33657-84-D-0165
Requester: FTD/TQTA
Approved for public release; distribution unlimited.

GRAPHICS DISCLAIMER

All figures, graphics, tables, equations, etc. merged into this translation were extracted from the best quality copy available.

A Comprehensive Analysis Algorithm for Ablation, Temperature Fields, and Thermal Stresses of Carbon-based Nosetip Materials

Huang Zhenzhong

ABSTRACT

This paper narrates the composite calculative principles for ablation, conduction, and thermal stresses of flight vehicles in a re-entry environment, as well as a few techniques beyond these principles. In regards to the chemical reactions of carbon-based material ablative surfaces, a selective calculation result is used to simplify the thermochemical ablation calculations. A spaced and non-spaced three-level explicit difference scheme was chosen for use in the calculation of temperature fields. Thermal stresses were calculated using the Finite Element Method within the Hypothesis of Linear Elasticity, based on the incomplete Principles of Variational Potential Energy, wherein it is possible to calculate the influences of many different types of displacement boundary conditions. During the compilation of the comprehensive analysis procedures herein, an automated mesh dividing technique was found which has application in selective calculations.

This document received November 12, 1982.

I. Foreword

The use of carbon-based materials to serve as heat shields in flight vehicles has long been a primary objective of research [1-3]. One of the leading reasons for this is to make thermal ablation an insignificant factor of external change that takes place during the time of re-entry. However, the abrupt thermal environment and subsequent onslaught of thermal stressors is a very serious danger. Resultingly, a comprehensive analysis algorithm that simultaneously calculates thermal environment, ablation, conduction, and thermal stress has been created, and, in regards to the problems of combating heat with carbon-based nosetip materials, has become a vital necessity. This paper recounts the calculation methodology, and although it is equally applicable for use with QIAO-type nosetips, the figures and examples provided are for the SAI-type nosetips [TN: transliterations for QIAO and SAI may also be pronounced as KE and SE respectively; literal translations for the romanization are jacket/case/coated for QIAO and shell for SAI].

The thermal stress state of heat resistant nosetips not only impinges upon the nosetip's construction and form, but also impinges upon the thermal environment, ablation, and changes that take place within an instantaneous heat field. These factors each have a mutual influence. Herein, we endeavor to fully link these factors together and realize a possible simulation of actual conditions.

$A(\varepsilon_{ij})$ 应变能密度

B 无因次烧蚀率

c 比热

$c_\theta=(\partial r/\partial\theta)_\phi$

$c_\phi=(\partial r/r\sin\theta\partial\phi)_\theta$

ε_{ij} 应变张量

$\gamma_c^{(i)}$ i 个反应中烧蚀的碳占总热化学烧蚀率的分数

f_i 体积力

H 焓

J 高度

$h_\xi=\Delta/(1+c_\theta^2+c_\phi^2)^{1/2}$, $h_\theta=r$, $h_\phi=r\sin\theta$

I 单位矩阵

J j 方向差分网格节点总数

k_ξ, k_θ, k_ζ 主方向的导热系数

L l 方向差分网格节点总数

m_w 总烧蚀率（指各反应的烧蚀率之和）

N_i, N_j, N_m 形函数

n_ξ, n_{r_c}, n_z 边界法线方向余弦

$\bar{P}_i$ 边界载荷

$q_{c,w}$ 进入烧蚀壁的热流

q_{r_e} 空气对壁面的辐射热

$q_{w_{光}}$ 光滑表面冷壁热流

q_{r_θ}, q_z 柱坐标的径向和轴向热流

q_ξ, q_θ, q_ϕ 变换坐标系内三个方向的热流

ΔQ_i i 个反应中单位质量的反应热

r 球坐标系内的径向坐标

r_c 柱坐标系内的径向坐标

R_0 端头初始曲率半径

r_i, r_j 球坐标系内的界面和物面径向坐标

s_p, s_u 载荷和位移边界

t 时间

T 温度

u 径向位移

u_i 位移向量

$\bar{u}_i$ 已知位移向量

v 轴向位移

w 周向应变

x, y, z 直角坐标轴

$\{\delta\}$ 以节点的 w、v 为待定参数的列向量

$\Delta=r_j-r_i$ 如图 3 所示

β 端头帽锥身半锥角

ε 辐射系数

θ 球坐标系内的方位角或位置向量与 z 轴的夹角

ξ 变换坐标

Π 泛函

ρ 密度

σ 波尔兹曼常数

σ_{ij} 应力张量

σ_r, σ_z, σ_θ 径向应力，轴向应力，周向应力

ϕ 球坐标方位角

ψ 附面层质量引射热堵塞因子

下 标

e 附面层外缘

j, l ξ 和 θ，或 z 和 r_c 方向的节点号

o 初条件

W 壁面

Table of Terminology

$A(e_{ij})$.....strain energy density

B.....dimensionless ablation rate

c.....specific heat

$c_\theta = (\partial r / \partial \theta)_\phi$

$c_\phi = (\partial r / r \sin\theta \partial \phi)_\theta$

e_{ij} .....strain tensor

$e_C^{(j)}$ .....fraction of total thermochemical ablation rate of carbon bases in ablative reaction

F_i .....volume force

? total heat

H .....height

? $= (1+c_\theta^2+c_\phi^2)^{1/2}$. $h_\theta = r$. $h_\phi = r \sin\theta$

I.....matrix unit

J.....difference of orientation J and sum of mesh points

k_a. k_b. k_c ..primary orientation of thermal coefficient

L.....Difference of orientation L and sum of mesh points

m_ω .....total ablation rate (ref to ablation rate of ea reaction)

N_i. N_j. N_m shape function

n_j. n_{re}. n_z cosine of normal boundary line orientation

P_i .....boundary load

$q_{\theta,n}$.....thermal current entering ablative wall

$q_{r\theta}$.....radiant atmospheric heat opposing ablative wall

q_r .....glossy surfaced, cold-walled thermal conductor

q_{re}. q_z ...radial and axial thermal conductivity of columnar coordinate

a_ξ, a_θ, a_ϕ orientations of thermal conductivity in varying coordinate system

ΔQ_i .....unit of thermal heat in reaction i

R_θ .....initial radius of nosetip curvature

r_i .....radial coordinates within spherical coordinate system

r .....radial coordinates within columnar coodrinate system

r_i, r_j ...radial coordinates of the spherical coordinate system

boundary and body surface

s_f, s_u ...load and displacement boundaries

t.....time

T.....temperature

u.....radial displacement

u_i .....displacement vector

$\bar{u}_i$ .....previously known displacement vector

v .....axial displacement

w.....circumferential stress

x,z ....right angle(d) coordinate axes

$\{\delta\}$ .....required parameter for ordered vector of specified node u,w

$\Delta = r_j - r_i$ as explained in Figure 3

β .....hemiconic angle for nosetip cone

ε .....radiation coefficient

θ .....orientation angle or positional vector of entry angle

of axis in spherical coordinate system

ξ .....varying coordinates

II.....functions

ρ .....density

σ .....Boltzmann Constant

σ_{ij}.....stress tensor

$\sigma_r, \sigma_z, \sigma_\theta$....radial stress, axial stress, circumferential stress

φ .....spherical coordinate azimuth

ψ .....blocking factor for qty of reflected thermal heat of attached surface layer

LESSER DESIGNATORS

e.....outer fringe of attached surface layer

j,i.....and . or z and r nodal designator direction

o.....initial conditions

W.....barrier wall surface

II. Ablation and Ablative Contour

During the course of re-entry, the carbon-based protective heat shield's thermochemical ablation primarily occurs at extreme surface temperatures that surpass 3000 degrees K. During this time, the carbon surface's thermochemical reaction can be expected to depart from normal theoretical conditions [4] [TN: sic]. The surface temperature of the heat resistant shield rises extremely fast during the time of re-entry, although during initial re-entry it is influenced by abnormal thermochemical reactions. However, for quantitative comparisons of total ablation, this particular stage of ablation is very limited. Nonetheless, during the time of actual re-entry, all calculations of ablation are in accordance with normal chemical hypotheses and could not lead to errors that would influence outcome of calculation [TN: sic].

The meticulous analysis conducted for thermochemical ablation of carbon-based nosetips uses thermodynamics data taken from bibliographical reference [5] [TN: the document cites reference 5 when, in fact, it is referring to reference 6!]. In regards to the thermodynamics numeric data provided for five types of vapors and 10 types of compounds: C (gaseous), C_2, C_3, C_4, C_5, CO, CO_2, C_2O, C_3O_2, CN, CN_2(C-N-N), CN_2(N-C-N), C_2N, C_3N_2, and C_4N_2, a dressing by screening calculation was conducted for actual ablative surface edges of the projectile. The results can be seen in Figure 1. Here, $f_c^{(i)}$ (i =1, 2, 3, ..., 15) expresses successive formation of the aforementioned compound reactions. Carbonization in ablative change occupies only a fraction of the total thermodynamic ablative rate. Calculations

clearly indicate that in an ablative carbon surface, the formation of CO, C_3, C_2N, and CN in a reaction (corresponding to $f_C^{(1)}$, $f_C^{(3)}$, $f_C^{(13)}$, and $f_C^{(14)}$'s curve in Figure 1), in regards to the carbon's ablation rate or the contributions of the thermal effect when compared to other reactions, is much larger. This fact alone could greatly simplify the calculation of ablation. It is sufficient for us to calculate these major reactions and corresponding chemical elements, so

$$3C \rightleftharpoons C_3$$

$$C + \frac{1}{2}O_2 \rightleftharpoons CO$$

$$C + \frac{1}{2}N_2 \rightleftharpoons CN$$

$$2C + \frac{1}{2}N_2 \rightleftharpoons C_2N_2$$

As the thermodynamic data clearly shows, in common ablative surface temperature ranges, the normal constants and thermal effects of these reactions can be completely expressed in Figure 1 with use of similar equations and approximation averages used as their expressions. This makes calculation of ablation much more convenient. The normal constant in a carbon-oxygen reaction can only use an oxygen residual that is equal to zero as a substitute. This is because from the normal constant we know that oxygen in an ablative reaction has an actual residual value that is so small we can consider it as negligible from the start.

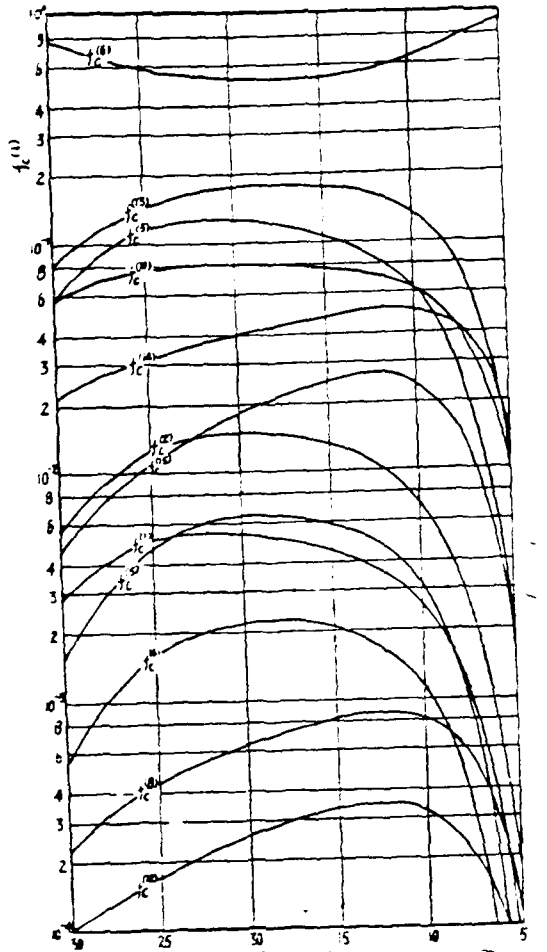

Figure 1. Various carbonic ablative rates for reactions at ablative wall represented as a fraction of projectile change.

The ablative wall's quantitative thermochemical ablative rate can be expressed as

$$m_{\omega} = B \cdot \psi q_{\omega *} / h_{\omega} \tag{1}$$

wherein the dimensionless ablative rate B is derived as a normal constant by means of a co-routine to figure the dispersion equation for the attached surface layer.

The thermal current entering the ablative wall is

$$q_{0,\omega} = \psi q_0 + q_{r,\omega} - \varepsilon \sigma T_w^4 \tag{2}$$

The second and third orders of the equation on the left represent the atmosphere opposing the ablative wall and the outer boundary radiant heat of the ablative wall. Furthermore,

$$q_e = q_{w*}\left[\left(1-\frac{h_w}{h_e}\right)+\frac{B}{h_e}\sum_i f_c^{(i)}\Delta Q_i\right] \tag{3}$$

We need only provide calculations for denudation and particle immersion, then we can perform a comprehensive calculation sequence for conduction and contour changes [TN: sic] as influences of thermal stress.

The nosetip, during the course of the ablative process, undergoes an instant exterior contour change, and this can be represented as an equation

$$\frac{\partial r_j}{\partial t} = -\frac{\Delta}{h_t|_{r=r_j}}\cdot\frac{m_w}{\rho} \tag{4}$$

Here, m_w is the quantative rate for ablation, denudation, and immersion [TN: particle immersion]. This is a nonlinear, hyperbolic differential equation. The methodology used in deriving this equation is first to begin with an approximation linearization equation, then use the Implicit Difference Scheme. This serves as a type of man-made patch that allows us to create a difference equation. Finally, we use a method of substitution to derive our solution. Bibliographical references [5, 7] iterate the process in precise detail. In Figure 4 at the back of this paper, a simultaneous calculation of temperature fields is outlined. These methods [TN: refers to above methods] are used to calculate the course of ablative heat protection for the nosetip contour.

Table 1. Approximation Formula for Normal Constants & Thermal Effect.

$\lg K_p = a - b \times 10^3/T(°K)$			$\Delta Q = c - d \times 10^{-3} T(°K)$	
Reaction Formulae	a	b	c	d
$3C \rightleftharpoons C_3$	9.541	39.284	199.7	5.31
$C + \frac{1}{2}O_2 \rightleftharpoons CO$			-23.8	2.11
$C + \frac{1}{2}N_2 \rightleftharpoons CN$	5.008	22.204	101.6	Ø
$2C + \frac{1}{2}N_2 \rightleftharpoons C_2N$	6.572	28.448	137.6	1.98

III. Instantaneous Temperature Fields

The majority of carbon-based materials assume an anistrophical form, and as a result of this we must conduct calculations by means of a thermal conduction equation for the anistrophic materials. In calculating the temperature fields for the SAI-fabricated nosetip model, we must break down the calculations for the SAI-model nosetip proper and the secondary components. For this, we will choose to use an arbitrary boundary surface. For example, a spherical surface which meets a man-made boundary as depicted in Figure 2. In regards to the main component, a spherical coordinate system was selected with the corresponding coordinate origins. Furthermore, a mobile coordinate system was used in conjunction with the ablation displacement boundaries so the below illustrated coordinate transformations could be carried out:

$$\xi = \frac{r - r_i}{\Delta(\theta, \phi, t)} \tag{5}$$

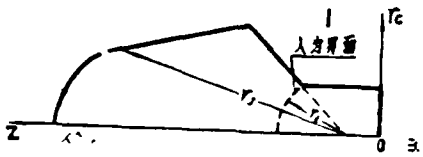

Figure 2. Coordinate System.

With the ablation displacement boundary transformation equations, we now have a stable boundary. Furthermore, thermal conductivity for the three mutually perpendicular primary angles is represented in the equation as

$$\frac{\partial(\rho CT)}{\partial t} + \frac{\partial}{\partial x}\left(k_x \frac{\partial T}{\partial x}\right) + \frac{\partial}{\partial y}\left(k_y \frac{\partial T}{\partial y}\right) + \frac{\partial}{\partial z}\left(k_z \frac{\partial T}{\partial z}\right) = 0 \tag{6}$$

which becomes

$$\frac{\partial(\rho CT)}{\partial t} - \frac{\xi}{\Delta}\frac{\partial \Delta}{\partial t}\frac{\partial(\rho CT)}{\partial \xi}$$

$$= -\left[\frac{1}{r^2}\frac{\partial}{\partial \xi}\left(\frac{r^2}{h_\xi}q_\xi\right) + \frac{1}{h_\theta \sin\theta}\frac{\partial}{\partial \theta}(r\Delta \sin\theta q_\theta) + \frac{1}{h_\phi r\Delta}\frac{\partial}{\partial \phi}(r\Delta q_\phi)\right] \qquad (7)$$

Here, $\partial\Delta/\partial t$ is the rate at which the width changes. This is from the external change rate $\partial r_s / \partial t$ from equation (4). Now the ablation boundary's thermal conductivity conditions are

$$\xi = 1, \quad \therefore \quad q_\xi = -Q \qquad (8)$$

and

$$Q = q_{0,\infty} + \rho\left(\int_{T_0}^{T_\infty} C dT\right)(1 + C_\theta^2 + C_\phi^2)^{-\frac{1}{2}}\frac{\partial \Delta}{\partial t} \qquad (9)$$

Now we need only check the zero angle of attack in the body of revolution. Furthermore, at the very minimum, we must also check the wind axis and the anistrophic similarities of the level surface. With the materials of $K_a = K_b$, we can cause a differential abatement involving ϕ and simplify the problem of symmetrical wind axes. In this type of problem with wind axis symmetry, after the change has occurred in equation (7), the derivatives of the temperature-to-space coordinates of the first and second order, and the thermal flow opposing these atmospheric coordinates, all have internal [TN: reference] points that have a second order precision in a centered difference equation. We can have a second order precision for both

pre and post differences. In regards to the derivative of time, the temperature field is obtained throught use of the DuFort-Frankel difference scheme. Afterwords, from the equation we get

$$T^{n}_{i,j}=\frac{1}{2}(T^{n+1}_{i,j}+T^{n-1}_{i,j})+0(\Delta t^{2}) \tag{10}$$

Here, superscript n represents the time gap. Omitting the minute quantities of higher order, we can correctly obtain a direct and simple calculation of stability using the three-level explicit difference equation. To follow along with the detailed process and reasoning of this equation, refer to bibliographical reference [5]. Therein, it provides an explanation on the precision and analyses for this, the algorithm which provides us with an excellent degree of precision and influences the time gap very little.

In regards to the SAI-model component, it is nonexistent in the displacement boundary. This is because a fixed columnar coordinate system was chosen for use. We also have a zero angle of attack in the body of revolution, so for $K_a = K_b$, the thermal conductivity equation can be written in axisymmetrical form as

$$\frac{\partial(\rho CT)}{\partial t}=\frac{1}{r_o}\frac{\partial}{\partial r_o}\left(r_o k_o \frac{\partial T}{\partial r_o}\right)+\frac{\partial}{\partial z}\left(k_o \frac{\partial T}{\partial z}\right) \tag{11}$$

for the main body of the SAI component. For the man-made boundaries of the SAI component, we must use a method of calculation that coordinates thermal flow calculations with the sequence of conditions that arise.

In carrying out our data analyses, we should point out a few facts for the use of the difference equation (11): speaking in terms of the θ coordinates within the spherical coordinate system, the main component is

partitioned into mesh lines based on averages. However, this mesh falls within the SAI component's columnar coordinate system and is represented as orientation r_c and its values are not based on averages. Furthermore, for the secondary boundary readings of thermal flow, this method sequenced the conditions in the proper order. The mesh points partitioned within the SAI component fall within this boundary and are, of course, calculated with the main component mesh points. This forced us to conform these mesh points to the non-spaced mesh points of the SAI component. At the same time, the boundary itself was also considered irregular. In order to coordinate this with the main component, for these types of non-spaced mesh points, a three-level explicit difference scheme must also be used. It is done by performing the Taylor spread on the origin node's temperature and thermal flow. By doing it in this manner, we get a derivative for temperature and thermal flow of non-spaced gaps for a difference approximation. For example,

$$\left(\frac{\partial T}{\partial r_e}\right)_{j,l}=\frac{1}{\Delta r_{ej,l}+\Delta r_{ej,l+1}}\left[\frac{\Delta r_{ej,l}}{\Delta r_{ej,l+1}}T_{j,l+1}+\left(\frac{\Delta r_{ej,l+1}}{\Delta r_{ej,l}}-\frac{\Delta r_{ej,l}}{\Delta r_{ej,l+1}}\right)T_{j,l}\right. \tag{12}$$

$$\left.-\frac{\Delta r_{ej,l+1}}{\Delta r_{ej,l}}T_{j,l+1}\right]+0(\Delta r_{ej,l}\cdot\Delta r_{ej,l+1})$$

$$\left[\frac{\partial}{\partial z}\left(k_e\frac{\partial T}{\partial z}\right)\right]_{j,l}=\frac{1}{\frac{1}{2}(\Delta z_{j,l}+\Delta z_{j+1,l})}\left\{\left(\frac{\Delta z_{j,l}}{\Delta z^2_{j+1,l}}k_{ej+\frac{1}{2},l}\right.\right.$$

$$+\frac{\Delta z_{j+1,l}-\Delta z_{j,l}}{\Delta z^2_{j+1,l}}k_{ej,l}\Big)T_{j+1,l}+\left(\frac{\Delta z_{j+1,l}}{\Delta z^2_{j,l}}k_{ej-\frac{1}{2},l}+\frac{\Delta z_{j,l}-\Delta z_{j+1,l}}{\Delta z^2_{j,l}}k_{ej,l}\right)T_{j-1,l}$$

$$-\left[\frac{\Delta z_{j,l}}{\Delta z^2_{j+1,l}}k_{ej+\frac{1}{2},l}+\frac{\Delta z_{j+1,l}}{\Delta z^2_{j,l}}k_{ej-\frac{1}{2},l}-\left(\frac{1}{\Delta z_{j,l}}-\frac{1}{\Delta z_{j+1,l}}\right)^2(\Delta z_{j,l}\right. \tag{13}$$

$$\left.\left.+\Delta z_{j+1,l})\,k_{ej,l}\right]T_{j,l}\right\}+0\left(\frac{\Delta z_{j,l}\cdot\Delta z_{j+1,l}}{\Delta z_{j,l}+\Delta z_{j+1,l}}\right)$$

and

$$\begin{cases}\Delta r_{ej,l}=r_{ej,l}-r_{ej,l-1}\\ \Delta z_{j,l}=z_{j,l}-z_{j-1,l}\end{cases} \tag{14}$$

Finally, we use a similar methodology for the non-spaced mesh points of the main component so we can get a non-spaced mesh point to be used in the three-level explicit difference scheme.

$$k_e \frac{\partial T}{\partial r_e} n_{r_e} + k_e \frac{\partial T}{\partial z} n_z = f(T, r_e, z, t) \qquad (15)$$

For the boundary conditions found at the irregular boundary, a very complicated difference scheme was constructed. This was due to the linear differences between mesh points and the boundary. Figure 3 provides an illustration of the boundary mesh points. We need a non-spaced difference expression for the temperature at node (J,l). Using a partial differential of the first order with second order precision, we must, at the same time, also have provisions for the intersection of the second order partial differential in the non-spaced difference equation. This establishes the difference equation for boundary conditions found in equation (15). Due to the use of a non-spaced difference approximation in the partial differential for the boundary, aside from the difference approximation differential itself, we must not rely too heavily on man-made approximations or else our results will not be as accurate [TN: sic].

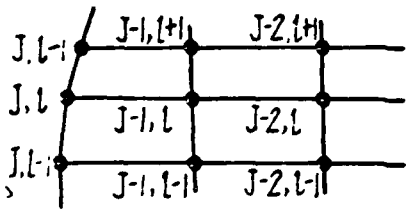

Figure 3. Mesh points (J,l) within the Mesh Point System.
a: n/a

It is in this manner that we realize a comprehensive analysis algorithm. The calculations shown are a model for spaced and non-spaced difference schemes. The time interval, stability, and precision are of little influence under these ordered conditions.

Figure 4 illustrates the calculation results for re-entry ablation and thermal conduction in a SAI-model graphite nosetip.

Figure 4. Calculation results for re-entry ablation and thermal conduction at varying altitudes for the SAI-model graphite nosetip.

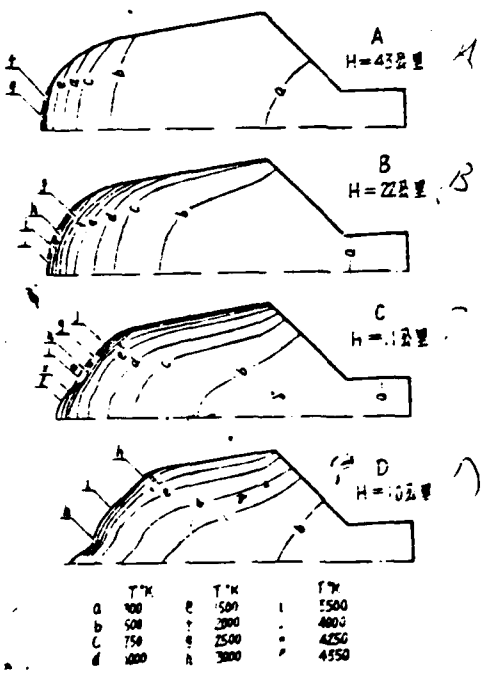

a: kilometers

b: kilometers

c: kilometers

d: kilometers

IV. Stress and Strain Fields

Carbon-type materials have a very small range of plasticity. Research in this area has been limited to problems dealing with strain and linear elasticity. In the fundamental calculations for known temperature fields, stress fields, and strain fields, this has been based on the incomplete Generalized Potential Energy Theory [8] and it fits into boundary load and boundary displacement conditions only in terms of the Principles of Linear Elasticity as related to minimal displacement

$$\Pi=\iiint_{V}[A(e_{ij})-F_i u_i]dv-\iint_{S_p}\bar{P}u_i ds - \iint_{S_u}(u_i-\bar{u}_i)\sigma_{ij}n_j ds \tag{16}$$

Here, the Finite Element Method was used to carry out the calculations. Within this equation, the subscripts i,j express the weight and summation sign. In problems of symmetrical axes, we can simplify values within the columnar coordinate system so our problem becomes one of a meridian surface. In the selection of a triangular form to become a finite element, aside from displacement τ at the axis orientation, the nodes are designated as constants. This causes the ablative surface shield to serve as the odd integral in the symmetrical axis. According to the proposals cited in bibliographical reference [9], we can directly obtain values for circumferential stress by

$$\frac{w}{\rho}=\frac{u}{r_0} \tag{17}$$

Within the singular element, we use the fabricated linearization to derive a value function

$$\begin{Bmatrix} w \\ v \end{Bmatrix}^e = [IN,\ IN,\ IN_n]\ \{\delta\}^e \qquad (18)$$

Here, the superscript e expresses a value for the singular element. $\{\delta\}^e$ is the ordered nodal constant previously ordered as

$$\{\delta\}^e = [w,\ v,\ \dot{w},\ v,\ \dot{w}_n\ v_n]^{eT} \qquad (19)$$

We use the extracted value function from equation (18) so we may have an integral for equation (16). Next, a similar extraction is done for the other elements forming a composite, overall functional. With an obtained numeric value equal to double the nodal totals, the unknown quantity is specified as nodal constants v and w which also gives a sub-equation for the symmetrical coefficient gap of linear elasticity. Based on this, we can obtain values for strain and stress from the strain-displacement and stress-strain derivatives.

In equation (16), because the boundary conditions are fully encompassed within the functional, this in no way causes illogical calculation of those boundary conditions. Moreover, we are still in the process of researching the effects produced for many different types and kinds of boundary conditions. In this aspect, we can only rationalize the sustained atmospheric pressure effects for the external boundary. However, the most important of all considerations, that of free boundary conditions, cannot be rationalized. This is a problem for which we must find a solution. In coming up with a proposal that meets all boundary conditions, it could possibly be broken into three conditions or categories for such an algorithm. The first would be for free boundary conditions; the second would be for pre and post boundary displacement, for example, dealing with pre-defined

displacement limit values of zero; the third could be for partial limits, for example, slippage angle loss allowances, exclusion of orientation displacement, etc. With these foundations, we can also, of course, very easily rationalize the co-existence or unity of the three aforementioned boundary conditions.

V. Selective Calculation Methodology

If, during the calculation of thermal stress, we calculate the nosetip contour at different points or origins, we must use the Finite Element Method to perform divisions for all of the prior mesh points, and this is indeed quite cumbersome. Even if we speak in terms of a single origin for the nosetip contour, because of ablation and the various conditions that are subject to change at any time, we still must be able to figure the origin of the nosetip contour at any instant, and all of these calculations are done using the Finite Element Method's long-hand division, performed one by one, by man, for each mesh point. This makes the whole process unfeasible. Because we can only perform calculations of thermal stress for a single, fixed form or for a few forms, each calculation must have its own division done one at a time. As a result of this, the development of an automatic mesh dividing technique for the physical contour changes that occur became a necessity. During the compilation of the comprehensive analysis algorithm, we discovered an automatic mesh dividing technique. By using this technique to perform the divisions in the Finite Element Method, not only can ablation changes be calculated for the physical contour, but the contour changes along the physical surface can be matched with these calculations. Furthermore, we need only specify the origins for the dimensions of the physical contour, then for different sized and shaped contours the automatic mesh dividing technique will perform the calculations and match things up. As expressed in Figure 5, after a suitable selection of the constants R_0, z_C, z_B, β, and θ_L, listed in the figure, we can carry out the calculations for each constant's physical changes in sequence by using the Finite Element Method.

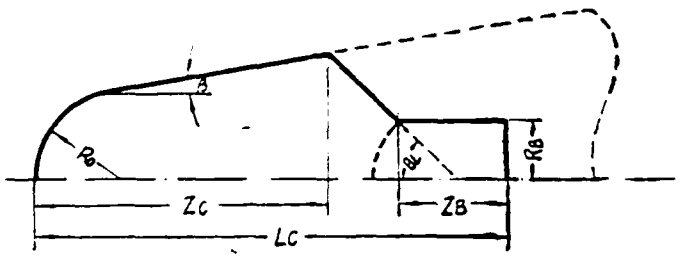

$$L_C = Z_C + \left(\frac{R_0}{\cos\beta} + (Z_C - R_0)\operatorname{tg}\beta - R_B\right)\operatorname{ctg}\theta_L + Z_B$$

Figure 5. Possible constants R_0, z_C, z_B, R_B, β, and θ_L for contour of SAI-model nosetip at initial stage.
n/a

Based on necessity, selection of these possible constants at different stages can greatly simplify the process of calculation. In the final quantitative analysis of the effects of various types of boundary conditions produced, this may provide significant contributions to engineering design.

In starting the comprehensive analysis algorithm for calculation during initial re-entry, based on the external constants provided for the thermal environment and the projectile type, we can begin to calculate ablation and the instantaneous temperature fields and the thermal environment as they are coupled together in real-time [TN:sic]. In fundamental calculations of the instantaneous contour for ablation, and for the instant temperature fields along the contour for changing boundary conditions, this method of calculation can provide for the stress and strain fields at any instant becuase of the automation of the mesh dividing technique for the Finite Element Method. We can use the algorithm to correctly calculate thermal flow with the following conditions:

Due to the calculation of temperature and contour at all times, the time intervals were set to a .2 second tolerance, and resultingly, all constants for calculations of the projectile are under these limitations.

The results calculated here for the constant $z_{\_}$, found in Figure 7 are only for the selective calculation results of a graphite nosetip.

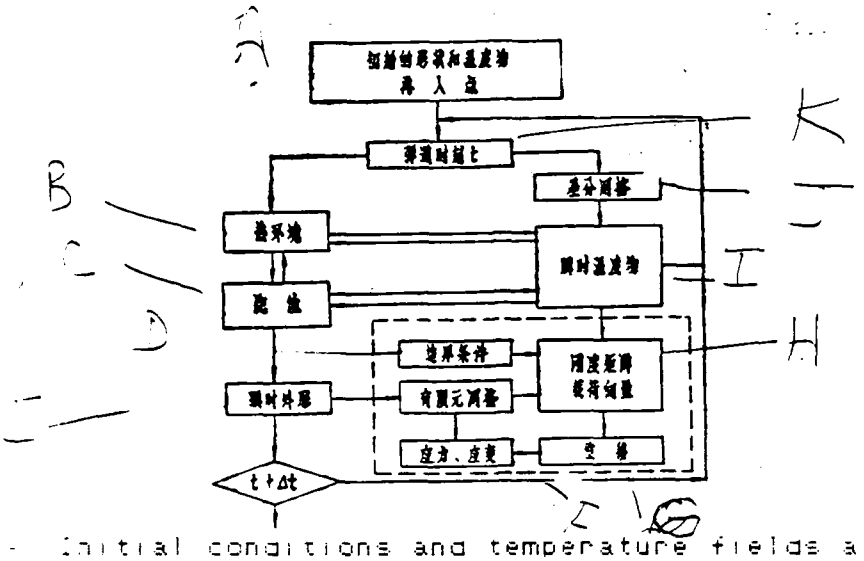

- Initial conditions and temperature fields at e-entry

b: illegible

c: illegible

d: illegible conditions

e: instantaneous contour

f: strain energy, strain tensor

g: displacement

h: illegible interval

i: instantaneous temperature field

j: mesh differences

k: time at projectile t

Figure 6. Flow of calculation.

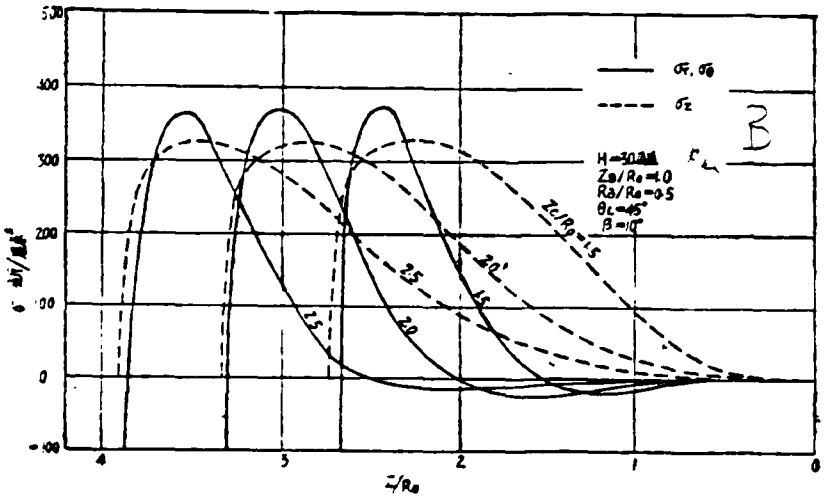

a: kg/cm^2

b: meters

Figure 7. Influence of strain distribution and axial

6. Conclusion

This paper iterated the comprehensive calculation algorithm for ablation, thermal environment, conduction, and thermal stress. Furthermore, within the comprehensive analysis algorithm, an automatic mesh dividing technique was tested. Utilization of the comprehensive analysis algorithm for carbon-based nosetips during re-entry ablation, conduction, and thermal stress at various atmospheric levels can be accomplished with comprehensive numeric data analysis. Moreover, the form and deterioration of the nosetip can be calculated in succession using selective calculation techniques [TN: sic].

Bibliography

[1] Segletes John A.: J. of Spacecraft & Rockets, 12, 1975.

[2] Chin, Jin H.: AIAAJ, 13, 1975, 5.

[3] Schneider, P. J., Teter, R. D., Coleman, W. D., Heath, R. M.: J. of Spacecraft & Rockets, 10, 1973, 9.

[4] Lundell, J. H., Dickey, R. R.: AIAAJ, 11, 1973, 2.

[5] Huang Zhenzhong: <<Journal of Aerodynamics>>, 1, 1981

[6] JANAF Thermochemical Tables, 2nd edi., NSRDS-NBS37. 1976.

[7] Cromwell, P. G.: SAMSO-TR-76-8.

[8] Xian Feichang: <<Experimental Mechanics>>, 1, 1979

[9] Xian Feichang: <<Applied Mathematics and Mechanics>>, 1, 1980

END

FILMED

1-86

DTIC